The evolution of He^+ irradiation-induced point defects and helium retention in nuclear graphite

Li, Mingyang; Shi, Chuanqing; Schut, Henk; Zhang, Zhengjun; Li, Zhengcao

DOI
10.1080/00223131.2019.1624654

Publication date
2019

Document Version
Final published version

Published in
Journal of Nuclear Science and Technology

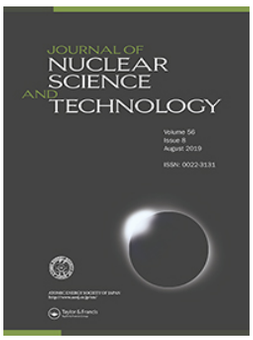

Journal of Nuclear Science and Technology

ISSN: 0022-3131 (Print) 1881-1248 (Online) Journal homepage: https://www.tandfonline.com/loi/tnst20

The evolution of He^+ irradiation-induced point defects and helium retention in nuclear graphite

Mingyang Li, Chuanqing Shi, Henk Schut, Zhengjun Zhang & Zhengcao Li

To cite this article: Mingyang Li, Chuanqing Shi, Henk Schut, Zhengjun Zhang & Zhengcao Li (2019) The evolution of He^+ irradiation-induced point defects and helium retention in nuclear graphite, Journal of Nuclear Science and Technology, 56:8, 744-751, DOI: 10.1080/00223131.2019.1624654

To link to this article: https://doi.org/10.1080/00223131.2019.1624654

JOURNAL OF NUCLEAR SCIENCE AND TECHNOLOGY
2019, VOL. 56, NO. 8, 744–751
https://doi.org/10.1080/00223131.2019.1624654

ARTICLE

The evolution of He^+ irradiation-induced point defects and helium retention in nuclear graphite

Mingyang Li[a,b], Chuanqing Shi[a], Henk Schut[c], Zhengjun Zhang[d] and Zhengcao Li[d]

[a]The State Key Laboratory of New Ceramics and Fine Processing, School of Materials Science and Engineering, Tsinghua University, Beijing, China; [b]Department of Engineering Physics, Tsinghua University, Beijing, China; [c]Department of Radiation Science and Technology, Delft University of Technology, Delft, The Netherlands; [d]Key Laboratory of Advanced Materials (MOE), School of Materials Science and Engineering, Tsinghua University, Beijing, China

ABSTRACT

The atomic-level study of point defect evolution in nuclear graphite is essential for a deep understanding of irradiation-induced property changes. The evolution of helium ion irradiation-induced point defects and helium retention in nuclear graphite ETU-10 and ETU-15 were studied by positron annihilation Doppler broadening (PADB) experiments and thermal desorption spectroscopy (TDS) measurements. The graphite samples were implanted with 10^{15}, 10^{16}, and 10^{17} cm^{-2} of 200 keV He^+ at operation temperatures below 373 K. Frenkel pairs were created during ion irradiation and they annihilated during annealing. Three stages of interstitial-monovacancy annihilation are suggested. At low temperatures, the initial annihilation would be refined only to the recombination of intimate metastable Frenkel pairs. When temperature increases, the annihilation would expand to a larger extent that isolate interstitials and vacancies annihilate with each other. In the case of high doses irradiation, vacancy clusters form at elevated temperatures. The retention and release of helium is tightly related to the evolution of the defects, especially the vacancies. The small over-pressured He-V clusters (He_nV) are thought to be the most possible form of helium retention under irradiation.

ARTICLE HISTORY
Received 21 February 2019
Accepted 19 May 2019

KEYWORDS
Nuclear graphite; point defect; positron annihilation; helium; irradiation

1. Introduction

Nuclear graphite refers to the graphite intended for application in nuclear reactors. Graphite has been used as the neutron moderator and structural material in several kinds of graphite-moderated nuclear fission reactors, including Magnox, Advanced Gas-cooled Reactor (AGR) and High-Temperature Gas-cooled Reactors (HTGR). The advantages of nuclear graphite include low neutron absorption cross section, high chemical purity, good thermal and mechanical properties at very high temperatures (>1000°C), good compatible with the other materials used in the reactor core, high chemical stability, and inexpensiveness, which enable nuclear graphite to be an important component in nuclear power plants [1–3]. However, Very High-Temperature Reactor (VHTR), which is a Generation IV reactor concept that comprises HTGR but with a potential core outlet temperature of at least 1273 K [4], has set higher demands to nuclear graphite [5–9]. In the moderation process, neutrons collide with carbon nuclei and thereby transfer kinetic energy to carbon matrix, and then the carbon atoms are knocked and will be displaced from their equilibrium positions and thus distort the surrounding lattices [10,11]. As a result of long-term neutron irradiation, the structure and properties of graphite would be seriously harmed, and the safety of nuclear power plants would be threatened by the failure of graphite components. Therefore, it is of great importance to study the response of graphite to radiation damage and to understand the defect behavior in thermal environment.

A lot of efforts have been made in this field, and most of the published work is focused on the microstructural changes and physical (elastic, thermal, electrical, magnetic) property variations of irradiated nuclear graphite [12–18]. For ion-implanted metals, much attention has been paid to the diffusion mechanism of defects, and a few forms of defect complexes have been suggested [19,20], while for nuclear graphite, it is accepted that the irradiation-induced displacement results in the generation of Frenkel pairs of interstitials and vacancies [21–26]. In this case, the interstitials (I) distribute in the interlayer space, while the vacancies (V) locate in the graphite planes as the absence of carbon atoms. Some research suggested that vacancies play a key role in the microscopic evolution of the defects [24,25,27,28]. Ewels et al. [29] adopted a first principles approach with AIMPRO code to study the interaction of interstitials and vacancies in a graphite supercell that was constituted by 64 atoms in irradiated graphite. Considering that the migration barrier of vacancies is a higher order than that of interstitials [30], they assumed a stationary V surrounded by an I at

CONTACT Zhengcao Li zcli@tsinghua.edu.cn Key Laboratory of Advanced Materials (MOE), School of Materials Science and Engineering, Tsinghua University, Beijing 100084, China

various sites, indicating that a metastable defect structure (an intimate I-V pair) or a Stone-Wales defect can be a possible product of the irradiation. Xu et al. [31] have suggested a phase transition from microcrystalline graphite to amorphous carbon resulted from irradiation-induced vacancy defects clustering accompanied by the disordered regions overlap. Defect evolution has also been studied in our previous work on C^+ implanted ETU-10 nuclear graphite, and it has been found that there are two annealing stages at 450 K and 700 K, and the vacancy complex can survive up to 1400 K [32].

Since the environment in the next generation of graphite reactors involves higher neutron dose, higher temperature, and stronger energy transfer, higher requirements for the performance of nuclear graphite have been set, and the microstructural changing mechanism of graphite must be understood. Therefore, the mechanism of point defect generation and evolution in graphite is an important issue and need to be further investigated.

This work aims to obtain a deeper understanding of the evolution of defects at the atomic scale. By combining positron annihilation Doppler broadening (PADB) and thermal desorption spectroscopy (TDS) methods, the evolution and recovery of point defects at different temperatures have been studied and three stages of interstitial-monovacancy annihilation are suggested. Considering the simultaneous diffusion of the implanted helium atoms, the behavior of retained helium in graphite is also discussed. We show that the release of helium corresponds to the recovery of point defects.

2. Experimental

2.1. He^+ irradiation

In this work, the behavior of irradiation-induced defects in isotropic graphite ETU-10 and ETU-15, which are designed to be the candidates as the moderator in VHTR, is studied. ETU-10 and ETU-15 are nuclear graphite produced by IBIDEN, CO., LTD. The physical properties of ETU-10 and ETU-15 are listed in Table 1. The most important difference between ETU-10 and ETU-15 is the difference in density. The specimens with a dimension of 10 mm × 10 mm × 2 mm were cut from graphite bulk and implanted with 10^{15}, 10^{16} and 10^{17} cm^{-2} of 200 keV He^+ at operation temperatures below 373 K. As for the TDS tests, specimens with dimensions of 2 mm × 2 mm × 2 mm were cut from the implanted samples to suit the desorption chamber.

2.2. PADB measurement with annealing

The PADB measurements with stepwise annealing were conducted on the variable energy positron (VEP) [33] beam facility at Delft University of Technology.

Table 1. Properties of ETU-10 and ETU-15 (data from the manufacturer).

Property	Unit	ETU-10	ETU-15
Apparent density	g cm^{-3}	1.75	1.84
Tensile strength	MPa	34.3	45.0
Thermal conductivity	W m^{-1} K^{-1}	104.4	120.0
Thermal expansion coefficient	10^{-6} K^{-1}	3.8	4.5
Ash content	ppm	<5	<5
Porosity	%	15	11

The PADB technique is based on the conservation of energy and momentum. Neglecting the momentum contribution of a thermalized positron, the annihilation of a hypothetical zero momentum electron results in the emission of two collinear 511 keV annihilation photons. In real materials, the electrons always carry some momenta; hence, energies of emitted photons disperse around the energy equal to m_0c^2. Here, m_0 is the mass of an electron or a positron (whose masses are equal), while c is the speed of light. The total mass of a hypothetical zero momentum electron and a positron transforms into the kinetic energy of the two emitted photons during annihilation, and each photon shares an energy of m_0c^2, which equals to 511 keV. Therefore, in an annihilation spectrum, this dispersion is observed as a (Doppler) broadening of the 511 keV photo-peak.

In the immediate vicinity of a defect, the electron density and electron momentum distribution deviate from those in the undisturbed matrix. Due to the missing positive-charged atom core, a vacancy-type defect acts as a trap for the positron. Moreover, the average electron density is lower in a vacancy-type defect, due to the relative absence of core electrons. As a consequence, a positron trapped in a vacancy-type defect has a higher probability to annihilate with a less energetic and low momentum valence electron, which can be observed as a less broadened annihilation peak. The well-accepted parameters for characterizing the Doppler broadening are the so-called *S(harpness)*- and *W(ing)*-parameters, introduced by MacKenzie [34]. The *S*-parameter, defined as the ratio of a central area to the total peak area of the 511 keV photo-peak, is sensitive to the annihilation of positrons with lower momentum conduction electrons. The *W*-parameter, defined as the proportion of the area of the peak wings to the total area, represents the annihilation of positrons with higher momentum core electrons. The width of the region defining the *S*-parameter is chosen close to 0.5. In this way, highest sensitivity to changes in the shape of the annihilation peak is obtained, making it sensitive to positrons annihilated at vacancy-type defects.

The VEP facility delivers a beam of monoenergetic positron with an intensity of 10^5 e^+ s^{-1} and a diameter of approximately 8 mm at the position of the sample. Positrons from a ^{22}Na source are thermalized in a micrometer thin tungsten foil placed in front of the source. The positrons escaping from

the opposite surface of the moderator foil are accelerated by a simple linear electrostatic accelerator to the desired implantation energy in the range between 0.1 and 25 keV. The relationship between mean implantation depth $\bar{z}$ of positrons and their energy E is described as $\bar{z} = \frac{\alpha}{\rho}E^n$, where α = 4.0 μg cm^{-2} keV$^{-1.62}$ is a material-independent constant, ρ is the density of the material, and the power index n = 1.62 [35,36]. Therefore, by adjusting the energy of positrons, depth profiling of vacancies can be obtained.

VEP device provides the condition for stepwise annealing studies. Placed in a vacuum chamber, the specimens were heated up to a 100-K higher annealing temperature and maintained for 5 min, then cooled down to room temperature naturally and PADB was performed in each step.

2.3. TDS tests

The TDS technique has been used to monitor the release of helium gas atoms from the implanted samples during ramp heating. The TDS measurement was performed on the DEGA desorption setup at Delft University of Technology. In order to reduce the background contribution caused by the adsorbed gas on the specimens and vacuum chamber walls, an overnight bake-out at a temperature of approximately 400 K was performed. During the TDS measurement, the samples were heated up to 1200 K at a constant ramping rate of 0.5 K s^{-1}, and the release of He was monitored using a Pfeiffer Quadrupole Mass spectrometer.

3. Results

3.1. Depth profiling of defects and the effect of annealing

Figures 1, 2, and 3 show the PADB *S*-parameter of He$^+$ implanted graphite annealed at successive temperatures as a function of positron implantation energy (bottom horizontal axis) and positron mean implantation depth $\bar{z}$ (upper horizontal axis). The full lines through the datapoint are the fitting outcome by VEPFIT [37] fitting procedure, which solves the one-dimensional steady-state positron diffusion equation taking into account the depth-dependent positron implantation profile trapping and annihilation, adopting a three-layer-model. The first layer is the surface-affected layer, where positron annihilation behavior is mainly affected by the near-surface modification but less influenced by irradiation-induced

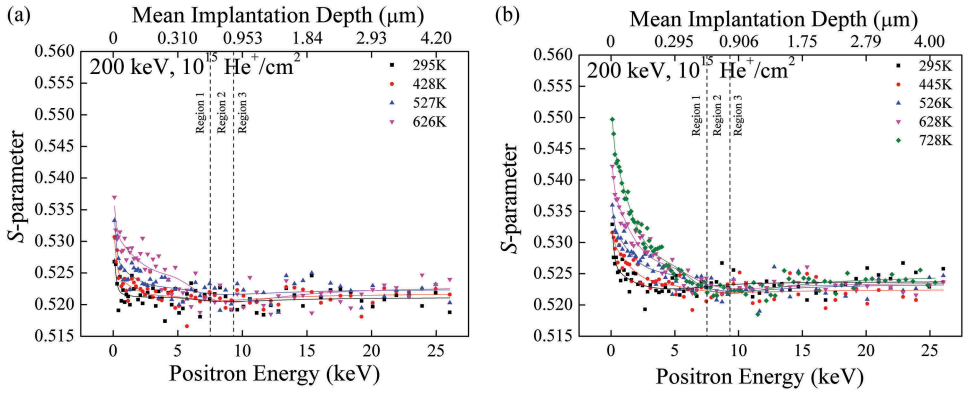

Figure 1. *S*-parameter of (a) ETU-10 and (b) ETU-15 implanted with 10^{15} He$^+$ cm^{-2} and annealed at successive temperatures as a function of positron energy in PADB tests.

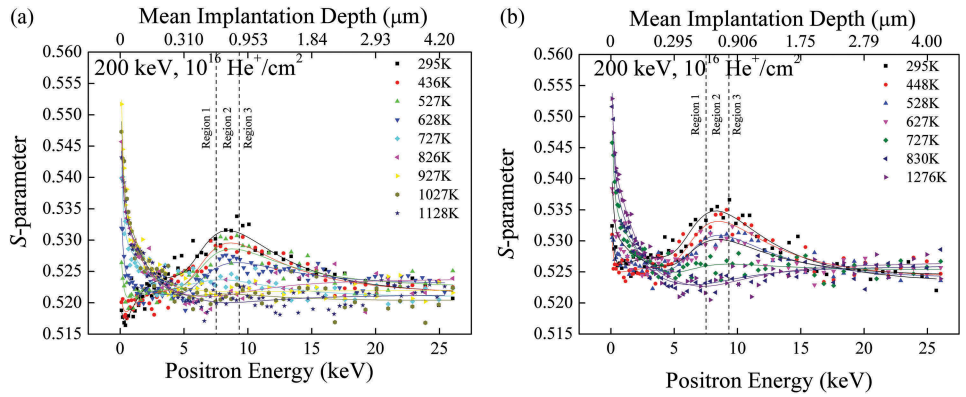

Figure 2. *S*-parameter of (a) ETU-10 and (b) ETU-15 implanted with 10^{16} He$^+$ cm^{-2} and annealed at successive temperatures as a function of positron energy in PADB tests.

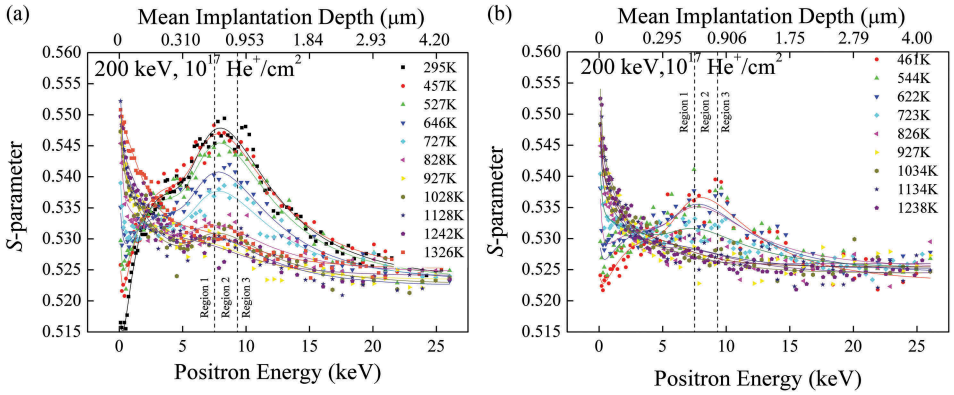

Figure 3. *S*-parameter of (a) ETU-10 and (b) ETU-15 implanted with 10^{17} He^+ cm^{-2} and annealed at successive temperatures as a function of positron energy in PADB tests.

defects [32]. The second layer is the region where most implanted He^+ ions stopped and a significant number of defects were induced, whose *S*-parameter is expected to be the most sensitive to ion irradiation. The third layer describes the remaining deeper region which is less influenced by ion implantation. The ranges of the first, the second and the third layer were calculated to be 0 ~ 600 nm, 600 ~ 850 nm and beyond 850 nm, respectively.

It is shown in Figure 1 that the *S*-parameters in ETU-10 and ETU-15 did not show the significant difference before and after annealing, implying that low dose implantation (10^{15} He^+ cm^{-2}), and subsequent annealing has little effect on the *S*-parameter. Since the amount of defects induced by irradiation is below the PADB sensitivity limit, which is approximately 1 vacancy in 10^6 atoms, it is inferred that 10^{15} He^+ cm^{-2} irradiation induced few vacancies in nuclear graphite. In the very near surface region (below 4 keV positron implantation energy) the effect of He^+ implantation is also not observed. The increase of *S*-parameter during annealing is likely due to the removal of shallow pre-existing defects introduced by sample preparation and surface modification giving rise to different electronic configuration and epithermal positron emission [38].

The PADB curves in Figures 2 and 3 show that prominent peaks appear in the 10^{16} and 10^{17} He^+ cm^{-2} implanted samples, and their maxima in Figures 2 and 3 are within the range from 600 to 850 nm depth. The depth profiles of vacancies in ETU-10 and ETU-15 were also calculated with SRIM 2013 code [39] with the displacement energy of 25 eV [40] and shown in Figure 4. The prediction of SRIM is that the vacancy peaks are going to be at almost 1 μm depth. It has been demonstrated that vacancy peak will appear at a shallower depth than the prediction of SRIM [41] because SRIM does not take the diffusion effect that the surface attracts vacancies into account. Therefore, the experimental results of PADB are reasonable. The effect of the increased dose is seen by the increase in *S*-parameter in Figures 2 and 3 for

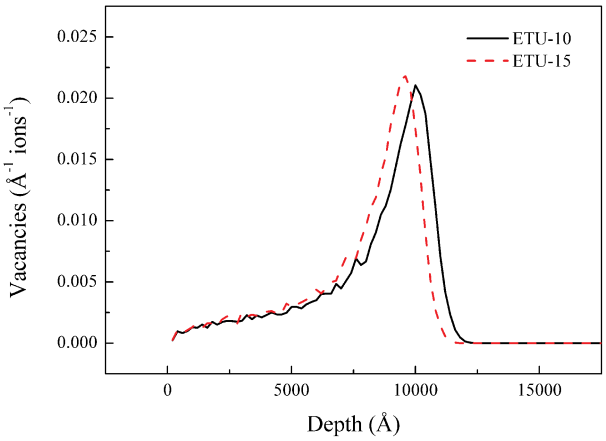

Figure 4. SRIM prediction of the depth profile of vacancies in ETU-10 and ETU-15.

the doses involved (10^{16} and 10^{17} He^+ cm^{-2}). This can be understood in two ways. A higher He^+ dose leads to a higher defect concentration under the same defect configuration. On the other hand, the formation of defects with larger volume (such as defect clusters, $V_{cluster}$) may also lead to the observed increase in *S*-parameter.

To further display the thermal evolution of the induced defects and determine whether vacancy clusters were introduced, the average *S*-parameter peak area values of the second layer (corresponding to positron energy ranging from 7.78 keV to 9.64 keV) are shown in Figure 5. The first point in every plot is the averaged *S*-parameter of the un-annealed irradiated samples. As can be seen, the *S*-parameter in 10^{15} He^+ cm^{-2} implanted ETU-10 and ETU-15 shows weak response to the stepwise annealing, indicating that only very few defects were introduced by irradiation at such a low dose.

After the 800 K annealing, the 10^{16} He^+ cm^{-2} implanted ETU-10 and ETU-15 have already recovered to the same level of *S*-parameters as the case of the 10^{15} He^+ cm^{-2} implanted ones. It is thereby concluded that defects induced by a relatively low dose can be removed

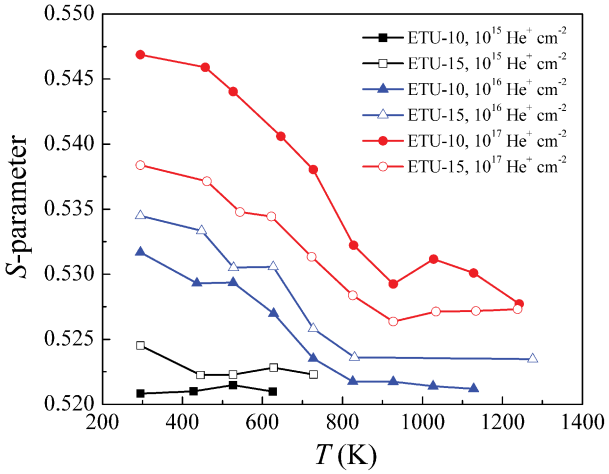

Figure 5. Average *S*-parameter values in the second layer of ETU-10 and ETU-15 as a function of annealing temperature.

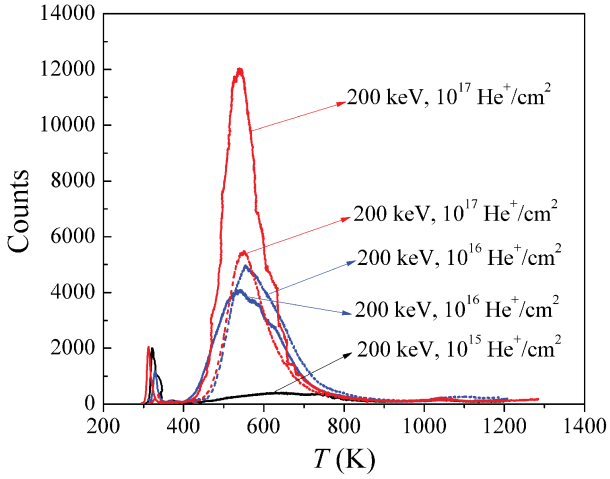

Figure 6. Thermal desorption spectra of helium of 200 keV He^+ implanted ETU-10.

by annealing. It is noticeable that the *S*-parameter values of ETU-15 are higher than that of ETU-10 at room temperature in cases of the low doses like 10^{15} He^+ cm^{-2} and 10^{16} He^+ cm^{-2}, while in the case of a high irradiation dose like 10^{17} He^+ cm^{-2}, the *S*-parameter of ETU-15 is much lower than that of ETU-10. Nevertheless, the comparison of *S*-parameter between different graphite grades cannot directly tell which material has better irradiation resistance. The higher density of ETU-15 may have led to the slighter increase of *S*-parameter after the same dose irradiation as ETU-10, but further experimental study should be performed on the dimensional change and mechanical and thermal property changes of ETU-10 and ETU-15 nuclear graphite after irradiation and annealing.

Another observation is that after the 1300 K annealing, the average *S*-parameter value in the case of 10^{17} He^+ cm^{-2} is still higher than the other two cases, which further indicates the above postulation that vacancy cluster formed.

3.2. Release of helium during annealing

The helium desorption spectra for ETU-10 are shown in Figure 6. For 10^{16} and 10^{17} He^+ cm^{-2} implanted samples, the results of two repeated tests are presented. The sharp spike at around 310 K is an artifact caused by switching on the filament [42]. Our discussion will focus on the temperature range from 400 to 1000 K, where well-resolved peaks are observed.

The peak intensity is found to be directly correlated with irradiation dosage. The signal of 10^{15} He^+ cm^{-2} implanted ETU-10 is very weak, inferring that only a small amount of helium retained in graphite after low dose implantation. This also explains why no defects (or at levels below the sensitivity limit) were introduced during the irradiation.

The release of helium starts at a temperature just above 400 K and reaches its maximum at about 550 K. Virtually, no desorption of helium has been observed at temperatures above 800 K. The 550 K TDS peaks of two 10^{17} He^+ cm^{-2} implanted samples are different in scale. Since the peak positions are the same, it can be inferred that they share the same mechanism of helium release. A possible explanation for the scalar difference is a spatial non-uniformity during the irradiation process, as the TDS samples were taken near the edges of the irradiated samples.

4. Discussion

4.1. Two stages of interstitial-monovacancy annihilation

As shown in Figures 2 and 3, the *S*-parameter values show almost the same variation tendency during the annealing from room temperature to 800 K, i.e. *S*-parameter gradually decreased to a relatively stable level. The decreasing *S*-parameters represent the reduction of positron traps, which is associated with the recombination and annihilation of Frenkel pairs. In graphite, interstitials are very mobile even at temperatures below 400 K, while the monovacancies become mobile only at elevated temperatures [10,28]. Therefore, the initial annihilation can be associated with the recombination of intimate Frenkel pairs [12]. Referring to the so-called Wigner energy, Mitchell et al. [43] and Ewels et al. [29] have reported that the characteristic peak at about 475 K can be attributed to the recombination of intimate Frenkel pairs, whose recombination into perfect graphite has a barrier of 1.3 eV to be overcome and releases 10.1 ~ 10.8 eV energy.

At elevated temperatures, the vacancies become mobile. Thrower et al. [44] found that the mobility of vacancies becomes significant above 673 K. Consequently, the annihilation of defects would expand to a larger extent at this stage when both isolate interstitials and vacancies can annihilate with any opposite point defect encountered. The long-range annihilation of

I-V recombination will dominate the annealing process when the temperature reaches 800 K. As suggested above, a hypothesis is proposed that the I-V annihilation in low-dose irradiated graphite can be divided into two stages according to the temperature dependence of the vacancy mobility.

4.2. Forming of vacancy clusters at high temperatures as the third stage

As shown in Figure 2, when annealing temperature was above 826 K (for ETU-10) or above 830 K (for ETU-15), the depth profiles of *S*-parameter in the 10^{16} He^+ cm^{-2} implanted samples did not have a further significant difference. Compared with Figure 1 (which shows that the stable *S*-parameter of 10^{15} He^+ cm^{-2} implanted ETU-10 and ETU-15 are 0.520 ~ 0.525), the *S*-parameters value of 10^{16} He^+ cm^{-2} implanted ETU-10 and ETU-15 after high-temperature annealing are almost the same, respectively. These observations collectively demonstrate that for 10^{16} He^+ cm^{-2} implanted graphite, almost all the defects can be removed and an almost full recovery can be expected after an annealing at 826 K (for ETU-10) or 830 K (for ETU-15) or higher temperatures.

However, as shown in Figure 5, even after annealing above 1200 K, the *S*-parameters in the 10^{17} He^+ cm^{-2} implanted samples retain a value notably above that of the 10^{15} or 10^{16} He^+ cm^{-2} implanted samples. It can be inferred that defect clusters that survive at 1242 K (for ETU-10) or 1238 K (for ETU-15) have formed in high-dose implanted ETU-10 and ETU-15. Because ion implantation has a maximum projection range, the very deep bulk region of the samples could not have been influenced by ion irradiation, and the deepest *S*-parameters can represent the un-implanted material. A similar phenomenon has been reported in our former work [32]. As shown in Figure 3, it is notable that the *S*-parameters of region 2 in the 10^{17} He^+ cm^{-2} implanted samples could not recover to the same level as their deepest bulk material, while in Figures 1 and 2 the *S*-parameters in region 2 did. These phenomena collectively demonstrate that the high-dose ion-irradiated samples cannot fully recover to the same level as un-irradiated materials.

It is reported that vacancies would become increasingly mobile above 873 K, forming stable vacancy clusters and therefore they are no longer available to recombine with the interstitials [45,46]. Thrower et al. [44] suggested that the interstitials themselves would first form clusters as the precursor of new graphene sheets, which then grow by trapping more migrating interstitials. They also found that at an annealing temperature above 900 K, point defects can develop into dislocation loops through migration. By the combination of positron annihilation technique and first-principle calculations, planar V_6 rings, which are a kind of aggregation of six vacancies that form a closed six-fold ring, have been approved to have high stability in irradiated graphite [47]. Calculations have demonstrated that the vacancy clusters are the most likely defect structure since they are energetically favorable and stable, which are suggested to be able to even survive the 1700 K annealing [47].

Given all the above discussion, for the 10^{17} He^+ cm^{-2} implanted ETU-10 and ETU-15, the defects evolution is suggested to go through three different stages under stepwise annealing. At first, when the temperature is as low as 400 ~ 500 K, the interstitials are mobile and the vacancies are immobile. As a result, the annihilation of point defects is restricted to the recombination of metastable Frenkel pairs, which is also an explanation for the well-studied Wigner energy release peak at 400 ~ 500 K [48]. Then at elevated temperatures, the vacancies become mobile (V_{mobile}); thus, isolate vacancies and interstitials would annihilate with each other in a larger extent, and the *S*-parameter gradually decreased to a stable level. In high-dose irradiated graphite, at 800 K, when the vacancies become fully mobile, vacancy clusters (vacancy sinks) form, and the annihilation of interstitials and monovacancies ceased [3]. This kind of new vacancy complex requires more energy to be removed. Only the first two stages are possible in the 10^{15} He^+ cm^{-2} and 10^{16} He^+ cm^{-2} implanted samples.

4.3. The state of helium retention

Based on the similarity of the spectra outlined in Figure 6, it is believed that helium atoms have the same release behavior and that only one form of He-V complex exists in the implanted samples.

Alimov et al. [49] found two maxima in the desorption spectroscopy and therefore assumed two different kinds of helium states in the graphite matrix. The first peak at 400 ~ 550 K was ascribed to the helium atoms released from the so-called 'solid solution' state, while the 650 ~ 800 K maximum can be explained by the gas escaping from the helium-filled bubbles. In Alimov's study, the 'solid solution' is assigned to helium atoms accumulated in the vacancy sites induced by irradiation. Since helium bubbles cannot be generated in irradiation doses lower than 10^{17} He^+ cm^{-2} [49], the only peak shown in this work should be ascribed to helium released from the 'solid solution' state.

Combined with the above discussion, at temperatures below 800 K, the dominant defect evolution during annealing is the annihilation of vacancies and interstitials. Moreover, the starting temperatures of the desorption of helium and the annihilation of vacancies and interstitials are roughly the same, which indicates that the TDS peaks in Figure 6 are tightly related to the defect evolution. Judging from the position of the helium release peaks during desorption, and taking into consideration the complexes that have been suggested in helium-implanted metal materials [19,20], the He-V complex is recognized as the small over-pressured He-V clusters

(He_nV, which refer to any small vacancy clusters that are filled with over-pressured helium), and it seems to be the most likely configuration of helium retention in He^+ implanted graphite.

These findings provide evidence that the in-plane vacancy diffusion mechanism may be a reasonable interpretation [50]. At temperatures just above 400 K, the evolution of induced defects starts from the annihilation of Frenkel pairs and helium atoms release from the He_n V clusters. At an elevated annealing temperature, the mobility of vacancies is greatly enhanced, and the recombination of Frenkel pairs becomes more intense, thus releasing more helium. At 550 K, the release of helium reaches its maximum. The decline of helium release beyond 550 K can be attributed to two reasons. One reason is the limited amount of retained helium atoms. The other reason is the generation of bigger vacancy clusters at elevated temperatures, where $V_{cluster}+V_{mobile}$ leads to a larger volume of vacancy and a lower helium pressure which is disadvantageous to helium release. Therefore, the helium release will decline until no further signal can be detected at temperatures above 800 K.

5. Conclusion

The evolution of the He^+ irradiation-induced point defects and helium retention in nuclear graphite ETU-10 and ETU-15 was studied by positron annihilation Doppler broadening (PADB) and thermal desorption spectroscopy (TDS) measurements and discussed. The main conclusions include:

(1) PADB results show that no sufficient defects were induced by 10^{15} He^+ cm^{-2} irradiation, while by increasing dose to 10^{16} and 10^{17} He^+ cm^{-2} irradiation-induced defects are observed. It agrees well with the widely accepted standpoint that Frenkel pairs are created during ion irradiation which annihilate during annealing.

(2) Three stages of annihilation processes were involved due to the temperature dependence of defects. Since the vacancies have low mobility at low temperatures, the initial annihilation is restricted to the recombination of the intimate metastable Frenkel pairs. At elevated temperatures, the vacancy becomes more mobile so the annihilation would expand to a larger extent, and the isolate interstitials and monovacancies can annihilate with each other. After annealing, a full recovery of defects can be expected in ETU-10 and ETU-15 implanted with low doses like 10^{16} He^+ cm^{-2}. As the third stage, in high dose (10^{17} He^+ cm^{-2}) implanted ETU-10 and ETU-15, vacancy clusters that survived at 1242 K (for ETU-10) or 1238 K (for ETU-15) form.

(3) The retention and release of helium is tightly related to the evolution of the defects, especially the vacancies. The small over-pressured He-V clusters (He_nV) are postulated as the most possible form of helium retention after irradiation.

Future work should focus on methods to efficiently remove the vacancy clusters, relieve irradiation induced damages and recover the property changes. The detailed mechanism of the diffusion of the gaseous atoms during the annealing should also be further studied.

Acknowledgments

This work was supported by the National Science and Technology Major Project of China [grant number 2011ZX06901-017] and [grant number 2008ZX06901-001], and the Koninklijke Nederlandse Akademie van Wetenschappen (KNAW) of the Netherlands. The authors thank Prof. Tadashi Maruyama of Ritsumeikan University (formerly of Tokyo Institute of Technology) for providing the graphite samples and their necessary information. The authors appreciate the anonymous reviewers for their helpful comments and suggestions. M Li thanks Dr Dongyue Chen of the University of Tokyo for useful discussion.

Disclosure statement

No potential conflict of interest was reported by the authors.

ORCID

Mingyang Li http://orcid.org/0000-0001-5973-7574
Zhengjun Zhang http://orcid.org/0000-0001-8727-6373
Zhengcao Li http://orcid.org/0000-0002-9899-5696

References

[1] Kelly BT. Physics of graphite. New York and London: Academic Press; 1962.
[2] Baker DE. Graphite as a neutron moderator and reflector material. Nucl Eng Des. 1971;14:413–444.
[3] Burchell TD. Nuclear graphite and radiation effects. In: Khj B, Cahn R, Flemings M, et al., editors. Encyclopedia of materials science & technology. Amsterdam: Elsevier; 2001. p. 6310–6319.
[4] Lee JJ, Ghosh TK, Loyalka SK. Oxidation rate of nuclear-grade graphite IG-110 in the kinetic regime for VHTR air ingress accident scenarios. J Nucl Mater. 2014;446:38–48.
[5] Yoon JH, Byun TS, Strizak JP, et al. Characterization of tensile strength and fracture toughness of nuclear graphite NBG-18 using subsize specimens. J Nucl Mater. 2011;412:315–320.
[6] Chi SH, Kim GC. Comparison of the oxidation rate and degree of graphitization of selected IG and NBG nuclear graphite grades. J Nucl Mater. 2008;381:9–14.
[7] Marrow J, Hodgkins A, Joyce M, et al. Damage nucleation in nuclear graphite. Energy Mater. 2006;1:167–170.
[8] Albers TL. High-temperature properties of nuclear graphite. J Eng Gas Turbines Power. 2009;131:064501.
[9] Kane J, Karthik C, Butt DP, et al. Microstructural characterization and pore structure analysis of nuclear graphite. J Nucl Mater. 2011;415:189–197.

[10] Burchell TD, Pappano PJ, Strizak JP. A study of the annealing behavior of neutron irradiated graphite. Carbon. 2011;49:3–10.
[11] Hinks JA, Haigh SJ, Greaves G, et al. Dynamic microstructural evolution of graphite under displacing irradiation. Carbon. 2014;68:273–284.
[12] Yang X, Xia H, Qin X, et al. Correlation between the vacancy defects and ferromagnetism in graphite. Carbon. 2009;47:1399–1406.
[13] Helm JW. Radiation-effects in graphite at high temperature. Carbon. 1966;3:493–501.
[14] Tanabe T. Radiation damage of graphite-degradation of material parameters and defect structures. Phys Scr. 1996;1996:7.
[15] Eapen J, Krishna R, Burchell TD, et al. Early damage mechanisms in nuclear grade graphite under irradiation. Mater Res Lett. 2014;2:43–50.
[16] Kim ES, Kim YW. Characterization of 3 MeV H^+ irradiation induced defects in nuclear grade graphite. Solid State Commun. 2010;150:1633–1636.
[17] Tsukuda M, Yokodera Y, Moritani K, et al. Heat treatment of graphite defects produced by irradiation with Ar cluster ions. e-J Surf Sci Nanotechnol. 2012;10:88–91.
[18] Zheng G, Xu P, Sridharan K, et al. Characterization of structural defects in nuclear graphite IG-110 and NBG-18. J Nucl Mater. 2014;446:193–199.
[19] Morishita K, Sugano R, Wirth BD, et al. Thermal stability of helium–vacancy clusters in iron. Nucl Instrum Methods B. 2003;202:76–81.
[20] Evans JH, Van Veen A, Caspers LM. The application of TEM to the study of helium cluster nucleation and growth in molybdenum at 300 K. Radiat Effic. 1983;78:105–120.
[21] Thrower PA. Interstitial and vacancy loops in graphite irradiated at high temperatures. Br J Appl Phys. 1964;15:1153.
[22] Urita K, Suenaga K, Sugai T, et al. In situ observation of thermal relaxation of interstitial-vacancy pair defects in a graphite gap. Phys Rev Lett. 2005;94:155502.
[23] Telling RH, Ewels CP, El-Barbary AA, et al. Wigner defects bridge the graphite gap. Nat Mater. 2003;2:333–337.
[24] Hjort M, Stafström S. Modeling vacancies in graphite via the Hückel method. Phys Rev B. 2000;61:14089.
[25] Hahn JR, Kang H. Vacancy and interstitial defects at graphite surfaces: scanning tunneling microscopic study of the structure, electronic property, and yield for ion-induced defect creation. Phys Rev B. 1999;60:6007.
[26] Pregler SK, Hayakawa T, Yasumatsu H, et al. Combined computational and experimental study of Ar beam induced defect formation in graphite. Nucl Instrum Meth B. 2007;262:240–248.
[27] Nordlund K, Keinonen J, Mattila T. Formation of ion irradiation induced small-scale defects on graphite surfaces. Phys Rev Lett. 1996;77:699–702.
[28] Latham CD, Heggie MI, Alatalo M, et al. The contribution made by lattice vacancies to the Wigner effect in radiation-damaged graphite. J Phys Condens Mat. 2013;25(13):135403.
[29] Ewels CP, Telling RH, El-Barbary AA, et al. Metastable Frenkel pair defect in graphite: source of Wigner energy? Phys Rev Lett. 2003;91:025505.
[30] Thrower PA, Mayer RM. Point defects and self-diffusion in graphite. Phys Status Solidi A. 1978;47:11–37.
[31] Xu HX, Lin J, J J L, et al. Characterization the microstructure and defects of matrix graphite irradiated with Xe ions. Nucl Instrum Meth B. 2017;406:638–642.
[32] Shi CQ, Schut H, Li ZC. Thermal annealing of C ion irradiation defects in nuclear graphite studied by positron annihilation. J Phys Conf Ser. 2016;674:012019.
[33] Schut H. A variable energy positron beam facility with application in materials science [Thesis]. Delft (The Netherlands): Delft University of Technology; 1990. Available from: http://resolver.tudelft.nl/uuid:d700e531-55d7-4f11-8488-18f81cac6748
[34] MacKenzie IK, Eady JA, Gingerich RR. The interaction between positrons and dislocations in copper and in an aluminum alloy. Phys Lett A. 1970;33:279–280.
[35] Vehanen A, Saarinen K, Hautojärvi P, et al. Profiling multilayer structures with monoenergetic positrons. Phys Rev B. 1987;35:4606–4610.
[36] Schultz PJ, Lynn KG. Interaction of positron beams with surfaces, thin films, and interfaces. Rev Mod Phys. 1988;60:701–779.
[37] Van Veen A, Schut H, Clement M, et al. VEPFIT applied to depth profiling problems. Appl Surf Sci. 1995;85:216–224.
[38] Carvalho I, Schut H, Fedorov A, et al. Helium implanted Eurofer97 characterized by positron beam Doppler broadening and thermal desorption spectroscopy. J Nucl Mater. 2013;442:377–381.
[39] Ziegler JF. [cited 2019 Jan 10] http://www.srim.org/
[40] Cartry G, Schiesko L, Hopf C, et al. Production of negative ions on graphite surface in H_2/D_2 plasmas: experiments and SRIM calculations. Phys Plasmas. 2012;19:063503.
[41] Shao L, Wei CC, Gigax J, et al. Effect of defect imbalance on void swelling distributions produced in pure iron irradiated with 3.5 MeV self-ions. J Nucl Mater. 2014;453:176–181.
[42] Hu Z, Li Z, Zhou Z, et al. Positron and thermal desorption studies on He ion implanted nuclear graphite. J Phys Conf Ser. 2014;505:012014.
[43] Mitchell EWJ, Taylor MR. Mechanism of stored-energy release at 200 °C in electron-irradiated graphite. Nature. 1965;208:638–641.
[44] Thrower PA. The study of defects in graphite by transmission electron microscopy. In: editor, Walker PL. Chemistry and physics of carbon: a series of advances. Vol. 5. New York: Dekker; 1969:217–319.
[45] Snead LL, Burchell TD, Katoh Y. Swelling of nuclear graphite and high quality carbon fiber composite under very high irradiation temperature. J Nucl Mater. 2008;381:55–61.
[46] Burchell TD, Snead LL. The effect of neutron irradiation damage on the properties of grade NBG-10 graphite. J Nucl Mater. 2007;371:18–27.
[47] Tang Z, Hasegawa M, Shimamura T, et al. Stable vacancy clusters in neutron-irradiated graphite: evidence for aggregations with a magic number. Phys Rev Lett. 1999;82:2532–2535.
[48] Latham CD, Heggie MI, Gámez JA, et al. The di-interstitial in graphite. J Phys Condens Mat. 2008;20:395220.
[49] Alimov VK, Scherzer BMU, Chernikov VN, et al. Helium reemission, desorption and microstructure evolution of graphites under helium ion implantation. J Appl Phys. 1995;78:137–148.
[50] Kaxiras E, Pandey KC. Energetics of defects and diffusion mechanisms in graphite. Phys Rev Lett. 1988;61:2693–2696.